Forecasting the Moisture Dynamics of a Landfill Capping System Comprising Different Geosynthetics: A NARX Neural Network Approach

S. M. Dassanayake[1], Ahmad Mousa[2], Gary J. Fowmes[3], S. Susilawati[2] , K. Zamara[4]

[1] Faculty of Business, Department of Decision Sciences, University of Moratuwa, Sri Lanka
[2] School of Engineering, Monash University Malaysia, Bandar Sunway, Malaysia
[3] School of Engineering, University of Warwick, Coventry, CV4 7AL, United Kingdom
[4] Tensar International Limited, Cunningham Court, Shadsworth Business Park, Blackburn, BB1 2QX, United Kingdom

Abstract

Engineered landfill capping systems consist of geosynthetics and soil layers, which often experience inconsistent and extreme weather events throughout their service life. Complex moisture dynamics in the capping layers can be created by these weather events in combination with other field conditions and can be detrimental to the system's integrity. The limited data on the hydraulic performance of landfill capping systems is a major challenge that hinders the development, validation, and calibration of models that can be used for realistic forecasting of these dynamics. Using the field-level data collected at the Bletchley landfill site, UK, this study develops a data-driven forecasting approach employing a non-linear autoregressive neural network with exogenous inputs (NARX). The data includes precipitation and volumetric water content (VWC) of the capping soil overlaying different geosynthetic layers recorded from Nov 2011 to July 2012. The NARX network was trained using the VWC data as inputs and precipitation data as the exogenous input. Also, the accuracy of NARX predictions was compared against that of a state-space statistical model. NARX-predicted VWC values for a period of 21-days ahead are distributed with a mean error of 0.05 and a standard deviation of 0.2. In the majority of prediction windows, NARX approach outperforms the state-space model. For all NARX prediction periods, $RMSEr$ has been less than 10% for the cuspated core geocomposite. Comparatively, $RMSEr$ values

increased to approximately 15% and 19% for the non-woven needle-punched geotextile and the non-woven needle-punched geotextile with band drains, respectively.

1 Introduction

Environmental concerns and economic considerations relating to potential failures of new and existing landfill capping systems have highlighted the need for optimized design and smart operation. The typical design of a landfill cap, which comprises a thin (0.3 to 2m) veneer of soil placed over a low permeability barrier layer, offers no prospect of monitoring the operational hydromechanical stability over its design life. Recorded failures of landfill capping systems involve elevated pore pressures and increased saturation levels in cover soils (e.g., Koerner and Soong, 2000; Jones and Dixon, 2003). However, little attention has been given to understanding the temporal variation of the moisture profile along the slopes of the cap above the low permeability liner. Due to the low confining stresses and the uncertain hydraulic boundary conditions in such capping systems, their integrity is highly susceptible to variations in the moisture and pore pressure distribution within the soil profile.

The impact of climate changes (e.g., UK climate change projections UKCP09, Murphy et al., 2009) on clay structures is critical – particularly when susceptible to high-intensity precipitation interspersed with dry periods. The changes in hydraulic conductivity and response to cyclic loading could be significant, depending on the soil's type and texture (Mousa and Youssef, 2019; Dassanayake and Mousa, 2022). Moreover, spatially concentrated heat spots in urban areas, known as the urban heat island effect (Senevirathne et al., 2021), can adversely affect the moisture transport within landfill structures (e.g., Plocoste et al., 2014; Menberg et al., 2013). Thus, there is a pressing need for robust and responsive predictive tools that can timely estimate the effects of weather changes on moisture dynamics in capping systems.

A limited number of studies have employed recorded field-level data to model the hydraulic performance (i.e., moisture dynamics) of operational landfill caps. Albright et al. (2006) and Henken-Mellies and Gartung (2004) built large-scale lysimeters on landfill caps in USA and Germany, respectively. The lysimeters monitor the water management of the caps and their hydraulic efficiency. Nyhan (2005) reports water balance parameters recorded throughout 7-years on a landfill site in New Mexico, USA. Additionally, numerical techniques like the finite element method have been used to estimate the stability of capping slopes within the scope of inflow-outflow boundary conditions (Narejo, 2013). Bussière et al. (2003) investigate numerical modeling software functionality through laboratory tests and site-derived data, focusing on capillary barrier effect and efficiency. Choo and Yanful (2000) compare predictions of the finite element simulations with laboratory test results. However, the numerical models require further improvements to consider a range of critical factors, such as evapotranspiration, multiple material types, three-dimensional slopes, unsaturated flow, and boundary conditions, for realistic forecasting of moisture transport regimes (e.g., Shukla and Kumar, 2008; Baah-Frempong and Shukla, 2018; Dassanayake and Mousa, 2020; Dassanayake et al., 2020; Dassanayake et al., 2021).

Data-driven modeling techniques, such as artificial neural networks (ANN), have shown potential for capturing the moisture-induced instability of the capping systems under simulated laboratory conditions. For example, Chao et al. (2021) show that different ANN models can capture the hydromechanical performance of soil-geocomposite drainage layer interfaces with significant accuracy. Additionally, Raja and Shukla (2021) employed well-established statistical indices and evidence from the literature to assess the predictive accuracy, sensitivity, and reliability of ANN models. However, insufficient field-level data collection programs have hindered the feasibility of developing ANN-based moisture forecast models for landfill capping systems.

2 Originality and Rationale

This study, as the first of its kind, uses a field-level dataset for a selected landfill capping system (data collected by Zamara et al., 2012) to closely study the relationship between the pore water pressure (PWP) distribution above the low permeability barrier within the system and cover stability, volumetric water content (VWC), and water balance parameters. The conducted analysis assesses the performance of different geosynthetic drainage products utilized in the capping system. It ultimately attempts to develop a robust ANN approach for forecasting the moisture migration of the system.

ANN typically processes data in several layers: one input layer, one-to-many hidden layers (HL), and one output layer. The conventional ANNs, known as feedforward networks (FFNs), achieve model convergence from information that flows only in one direction: forward iterations toward the output layer. Comparatively, ANNs, referred to as recurrent neural networks (RNNs), have feedback connections that enable information to flow in both forward and backward directions. A particular type of RNNs, known as non-linear autoregressive neural networks with exogenous inputs (NARX) (Leontaritis and Billings, 1985; Samarasinghe, 2016), uses additional information derived from the exogenous inputs (e.g., precipitation heights) to converge for the optimum prediction model rapidly. The use of additional input reduces the number of iterations and parameters needed to calibrate the NARX model. Such an approach effectively captures the complex (non-linear) dynamics, e.g., seasonal components, found in the time series of hydrogeological applications (e.g., Nanda et al., 2016; Guzman et al., 2017; Wunsch et al., 2018; Di Nunno et al., 2020; Di Nunno et al., 2021). Given the latency between the weather events and ground response, which can exhibit highly non-linear trends, this paper employs NARX architecture to support the forward prediction of the VWC variations in the landfill cap subjected to antecedent precipitation.

The performance of the NARX-based VWC predictions was statistically compared to that of an equivalent state-space process model to gauge the applicability of the presented approach. A state-space process model can be routinely used to analyze the measurements (or observations) obtained for stochastic and deterministic dynamical systems. To this end, the model can capture the performance of porous structures (analogous to landfill capping systems) that facilitate fluid flow (e.g., Gildin and Lopez, 2011; Zhu et al., 2020; Van Doren et al., 2008). It is a hierarchical model with a structure that accommodates the modeling of two-time series: (1) a state or process (precipitation measurements) and (2) an observation time series (VWC measurements). The structure of the model significantly differentiates process variation (i.e., precipitation variations) from the observation error caused by the randomness or imprecision in the VWC measurements. Since the VWC in a landfill cap varies following a stochastic dynamical process influenced by a series of precipitation events, the state-space model is suitable for independently forecasting the VWC variations.

3 Trial Sections

The trial sections were built in August 2011. The construction comprises the preparation of the clay barrier and installing different capping systems, installation of the geosynthetic panels, followed by the placement of the restoration soils **(Fig. 1)**. As shown in **Fig. 1b**, the first geosynthetic panel, GS3, was installed from the left, then GS2, and to the right is GS1. The control panel (soil only) was installed between panels GS3 and GS2. Field monitoring program

Fig. 1. *Trial sections: a) top surface of the clay barrier; b) installation of the geosynthetic panels; c) spreading the restoration soils; d) completed soil restoration.*

The data on the hydraulic conditions within a landfill cap was obtained from field monitoring at the Bletchley Landfill, Buckinghamshire, UK. The lining system comprises a compacted clay layer with geosynthetic inclusions and restoration soil. The field trial included four monitoring sections, three types of geosynthetic drainage layers, and one control section without a drainage layer installed. Dedicated field instrumentations allowed continuous measurement of the volumetric water content across the restoration soil layer thickness and pressure head at the interface between the restoration soils and geosynthetic drainage layers (Zamara et al., 2012). Discharge of water from the geosynthetic drainage layers was also monitored. Attempts to measure water run-of were undertaken; however, these were not entirely successful as detailed by Zamara et al. (2012). Weather station installations near the site provided accurate records of precipitation.

The site comprises a 1m compacted clay layer, 1×10^{-9} m/s (the barrier layer), overlain by cover soils. The geosynthetics, in addition to the regulated cap, did not form part of the permitted barrier at the site. In the instrumentation locations, the capping system comprised (from the bottom up) a compacted clay layer, a geosynthetic drainage material overlain by restoration soils. The trials replicate design solutions typically utilized for landfill capping systems. Different geosynthetics have been used to allow testing a range of capping configurations for this site. The ambient temperature was collected by a logger installed at the surface of the geosynthetics. The slope of the cover was uniform, with a gentle inclination angle of 1V:8H (7.1°). The instrumented sections of the cover (restoration soils) had a width of 5 to 6 m and a length of 40 to 45 m. Three different geosynthetic drainage layers were installed at the interface between the clay barrier and restoration soils (Fig. 2):

(a) Non-woven needle-punched geotextile (GS1)

(b) Geocomposite drainage layer, non-woven geotextile upper filter geotextile over a cuspated core (GS2)

(c) Non-woven, needle-punched geotextile with integral longitudinal band drains, wrapped in filter geotextile, at regular centers (GS3).

Fig. 2. *Geosynthetics used in the trials: a) GS1; non-woven needle-punched geotextile; b) GS2; cuspated core geocomposite; c) GS3; non-woven, needle-punched geotextile with integral longitudinal band drains at regular centers. (www.geofabrics.com).*

A control section without drainage was also instrumented for reference. The hydraulic parameters of the drainage materials are presented in **Table 1** (after Zamara *et al.* 2012). The relative performance of the drainage geosynthetics is discussed in Zamara et al. (2014). GS1 was a needle punch non-woven geotextile marketed primarily for protection applications. GS2 and GS2 were continuous geocomposites with band drains and in-plane flow capacities of 2.0 and 0.2 l/m/s under a 1m head at 20kPa confining stress (EN ISO 11058:2012).

Table 1. *Hydraulic properties of the geosynthetic layers.*

The restoration soils consist of site-won silty clays. The construction permit does not require compaction. However, soil placement was performed using a D6 Bulldozer, and thus induced compaction occurred through placement. The average thickness of the soil cover over the drainage materials is 0.4m. Permeability of restoration soils was estimated in laboratory conditions and on-site conditions. The permeability was tested in a triaxial cell (BS 1377:1990 Part 6, Method 6). The average coefficient of hydraulic conductivity for remolded soil samples was approximately 10^{-8} m/s, which caused a very slow migration of the moisture front through the capping soil layer. However, the drainage layer was responsive to precipitation events within a relatively short period of time (minutes, hours). In-situ measurements using a double ring infiltrometer (ASTM D3385-03) were carried out using an infiltrometer to better assess the soil permeability. The estimated in-situ coefficient of hydraulic conductivity through the desiccated structure of the recompacted soil was, however, in the order of 10^{-5} m/s. The properties of these soils are given in **Table 2** (after Zamara et al. 2012). Whilst the 1V: 8H slopes were used in the case study, the model could be equally applied to steeper slopes. The collected data set is relatively limited; however, it is hoped that demonstrating value to such data encourages the routine collection of a wider data range in the future.

Table 2. *Parameters of the restoration soil.*

Sixteen volumetric water content (VWC) reflectometers (Campbell Scientific CS616) were installed across the cap to detect the moisture movement along the slope, and across the soil layer. **Fig. 3** presents the installation process of the VWC sensors and the logging station.

Fig. 3. *Installation of VWC sensors in one of the selected locations: (a) two sensors installed at two different levels of the restoration soils capping; (b) logging station.*

The collected moisture can portray an idea about the soil's VWC response to weather conditions. The sensors were installed parallel to the slope at various depths in the restoration soil above the geosynthetics and clay barrier layer. The locations of the sensors relative to the slope crest and within the restoration soil column are given in **Fig. 4a.** The sensors were placed in the capping soil above the geocomposite liners and control section at approximately equal distances (**Fig. 4b**). They were logged every half hour.

Fig. 4*. Volumetric water content (VWC) sensors within the capping system: a) location; b) profile (depth in m). (after Zamara et al. 2012).*

Fig. 5 shows the recorded VWC measurements for each sensor depicted against the precipitation (blue color bars). A weather station located near the site was used for this purpose. The bottom and top sensors for any layer, X, have been denoted by X-38m and X-20m, respectively. Since the VWC data were recorded at half-hour intervals, the seven-day rolling average values have been generated to minimize the noise and showed prompt responses of the VWC sensors to precipitation events.

Fig. 5*. VWC and precipitation (h) data acquired over the study period (254 days)*

The sensors were installed in early November 2011. After nearly two weeks of installation, the VWC profiles have rapidly built up in response to a series of precipitation events (**Fig. 5**). The modest inclination of the slope has allowed most of the water to infiltrate into the cap during the precipitation events. However, the high VWC values remain approximately constant throughout the winter in the UK (November to March). As the climate becomes more temperate in April, the average of the recorded VWC values has slightly increased. The evapotranspiration has likely resulted in upward moisture migration and retention in the restoration soil.

The highest moisture content was observed at the GS2 bottom sensor (i.e., GS2-38m). Despite the cuspated drainage core, it is believed the presence of the polymeric sheet below and or the nature of the associated filter geotextile resulted in greater water retention of GS2. Compared to the two other geosynthetic configurations, the restoration soil above GS1 shows a lower VWC, with water appearing to wick along the geotextile. The sensor readings for GS2-20m and soil (control case) show almost identical VWC trends throughout the winter. Similarly, GS3-38 and GS1-20, and the sensors located between band drains (GS3) and soil show similar trends, particularly during precipitation events. The precipitation and dry periods have evidently induced complex VWC variations in the restoration soil capping. The largest fluctuations are shown in VWC for GS1-38m. It's position lower down the slope means more water is likely to migrate to this area of the slopes. The proximity to the drain could allow easier drainage resulting in a less steady state VWC; however, it is acknowledged that this is a natural capping system with low confinement clay layers. This may simply be a result of fracture flow through desiccated clays.

4 NARX Forecasting Model

The NARX network architecture was trained as an FFN using the target VWC values (Fig. 6) and exogenous inputs (i.e., precipitation values). The unknown VWC values were predicted using the RNN form. The FFN training was referred to as "open-loop architecture" (also known as "series-parallel"). The RNN prediction was termed the "closed-loop architecture" (Fig. 6). Open-loop training gave a greater calibration accuracy to the network due to the availability of the target values (VWC measurements).

Fig.6. *NARX model with one hidden layer and three hidden nodes, one input time series (h_t), transformed h_t values ($\underline{h}_t$), one output time series (VWC_t), and the feedback loop (activated in closed-loop architecture for multi-step predictions).*

4.1 Network architecture

The daily precipitation height (h_t) and 3-day rolling averages of the VWC values (VWC_t) were taken as the exogenous input and output (feedback), respectively. The collected h_t data were normalized considering the minimum and maximum height values for transformation to the [0,1] range (min-max transformation). Transforming h_t improves the convergence rate during the NARX training stage. Similarly, the 3-day rolling average taken for VWC_t minimizes the dispersion of the measurement errors under erratic field conditions while improving the smoothness of the time series. Equation 1 shows the transformed precipitation heights ($\underline{h}_t$) and the VWC values using the common definition for the NARX model.

$$VWC_t = f(\underline{h}_{t-1}, \underline{h}_{t-2}, \dots, \underline{h}_{t-n_x}, VWC_{t-1}, VWC_{t-2}, \dots, VWC_{t-n_y}) \quad (1)$$

where n_x and n_y represent the number of input and output layers, respectively. The FFN training conducted using the open-loop form can approximate the non-linear function, f. The NARX open-loop training comprises a specific number of user-defined hidden nodes and randomly selected values for the weights with fixed connections. During the training, forward iterations calibrate the weights to match the feedback VWC_t values using a set of prior VWC_t and h_t values. The training was conducted using the Levenberg-Marquardt (LM) algorithm. As an efficient and reliable second-order local optimization technique (Adamowski and Chan, 2011), LM encompasses the benefits of both steepest descent (first-order) and Gauss-Newton (second-order) methods (Samarasinghe, 2016). To this end, LM permits an improved calculation speed and stability compared to the steepest descent and Gauss-Newton techniques (Samarasinghe, 2016). Equation 2 shows the general weight update for epoch $n + 1$ in LM training (Yu and Wilamowski, 2018).

$$w_{n+1} = w_n - (H_n + \lambda I)^{-1} j_n r_n \tag{2}$$

At the epoch "n", w_n is the weight vector, H is the Hessian matrix, λ is a scalar variable, j represents the Jacobian matrix, and r is the residual error vector. The training procedure should be repeated several times on models with different numbers of hidden neurons, input delays (ID), and feedback delays (FD) to determine the NARX structure. The available number of training samples (N) can be used empirically to define the maximum number of hidden neurons (HN_{max}) as follows (after Wanas *et al.*, 1998):

$$HN_{max} = \lceil N \rceil \tag{3}$$

The ID and FD values can be introduced to represent the residual "short-term memory" of the non-linear system to the NARX network. Before the training stage, estimating these delays improves the prediction accuracy while minimizing the network size and training time. The boundaries of these values can be empirically determined after analyzing the autocorrelation of the input and output time series data. As given in Equation 4, autocorrelation is defined as the correlation between any two values of the time series (e.g., y_t and y_{t+1}).

$$Autocorrelation = \frac{COV(y_t, y_{t+1})}{\sqrt{VAR(y_t)VAR(y_{t+1})}} \tag{4}$$

Fig. 7 shows the autocorrelation graphs of the precipitation data and VWC values recorded by the three bottom sensors (GS1, GS2, and GS3) above the geocomposite layers. The autocorrelation of the precipitation data is greater than the sensor data. The trends suggest reasonable upper bounds for ID and FD of 10 and less than 5, respectively. Subsequently, a range of FD and ID values (from 1 to 10) was tested with different hidden layer sizes to determine the optimum network architecture based on the training performance. The Matlab® Neural Network Toolbox™ (MathWorks® Inc., 2020) was used to create and simulate the NARX models.

***Fig. 7**. Autocorrelation of the precipitation and VWC data recorded by the lower sensors (38m below the surface) with 10% confidence interval: a) precipitation data; b) GS1 composite; c) GS2 composite; d) GS3 composite.*

4.2 Network training and validation

The NARX network was trained in the open-loop architecture, and the predictions were made using the closed-loop architecture. In the training stage, both the input and output values were divided into three sets: the data points from 21 November 2011 to 4 May 2012 (set 1: 165 data points), 3 June 2012 (set 2: 198 data points), and 4 July 2012 (set 3: 229 data points). Each set was again partitioned into two subsets, following the typical 70–30% training-to-testing separation method (e.g., Samarasinghe 2016; Wunsch *et al.*, 2018). For instance, in set 1, data from 21 November 2011 to 14 March 2012 were used as the training data set and the remaining data was used to test the prediction accuracy of the model. The typical time series forecasting uses the last part of the data (approx. 10–15%) series to test for the network's prediction accuracy and generalization ability (Bergmeir and Benítez, 2012; Maier et al, 2010). At least 90% of the original data was used for model building, and the remaining 10% was employed for error calculation. Initially, set 1 (~65% of the total data) was incorporated into training and validating the model. In the next stage, set 2 (~78% of the total data) and set 3 (~90% of the total data) were used for the training and testing, respectively.

The model was completely rebuilt 10 times for each data set with different ID, FD, and HL numbers to avoid double usage of data for training and testing purposes. It is worth noting that the training data set is additionally divided into three subsets for model building. This approach enabled the software to perform early stopping during the open-loop training and thus effectively avoided overfitting. As such, for a given number of HL, a total of 3,000 open-loop simulations were performed, and the relative error (Equation 5) for the predictions was averaged (e.g., Bergmeir and Benítez, 2012; Bergmeir *et al.*, 2014) to decide the optimum network architecture. **Fig. 8** summarizes the prediction accuracy of 12,000 open-loop network simulations. The optimum performance of the NARX network was observed for an HL size of 3 with ID and FD of 4. This optimum network architecture was chosen to perform the closed-loop predictions. The mean percentage error (MPE) was used to assess the performance of the performed prediction. MPE is expressed as follows:

$$MPE = \left(\sum_{i=i}^{n} \frac{VWC_{i,observed} - VWC_{i,predicted}}{VWC_{i,observed}}\right) \frac{100\%}{n} \tag{5}$$

Fig. 8*. Average MPE of the prediction performance of the open-loop training by different NARX architectures (the crossed cells indicate an MPE greater than 10%).*

5 State-Space Predective Model

The performance of the NARX predictions was statistically compared to that of an equivalent state-space process model. The model is typically used for analyzing stochastic and deterministic dynamical systems that are measured (or observed) through a stochastic process (Shumway et al., 2000). A state process is also known as a Markov process in which the future state (e.g., a precipitation height, h_j measured at any future time, j $\{h_j : j > t\}$) and the past state (e.g., a precipitation height, h_i measured at any prior time, i $\{h_i : i < t\}$) are independent of the present state: a precipitation height, h_t made at time t. As shown in Equations 6 and 7, the state-space model is built around a state vector $q(t)$ comprising a series of stochastic parameters that linearly relate the degree of variation in input values. As shown in Equation 6, the state equation of the system is a linear combination of the state vector, state matrix (A), input matrix (B), and external input vector $h(t)$. Equation 7 defines the output equation where the output matrix (C) describes how the state-space values are combined to get the output VWC values, and the D is the direct transition matrix that is used to allow the inputs to bypass the system altogether and feedforward to the output.

$$\dot{q}(t) = \; Aq(t) + Bh(t) \tag{6}$$

$$VWC(t) = \; Cq(t) + Dh(t) \tag{7}$$

Both input and output vectors contain the corresponding values recorded at discrete time steps of a day. The state matrix, A, describes the underlying dynamics of the system and how the internal states are all connected. The input matrix, B, describes how the inputs enter the system. Similar to the NARX input and output data set, the developed state-space model is assigned the daily precipitation height h_t values as the input and the 3-day rolling averages of the VWC values (VWC_t) as exogenous output.

The performance of both the NARX network and state-space model has been evaluated using standard error indices: root mean squared error ($RMSE$), relative root mean squared error ($RMSE_r$), and the coefficient of determination (R^2) (Equations 8-10). The $RMSE$ calculates the error variance independently from the sample size. The $RMSE_r$ assesses absolute $RMSE$ values (Khalil *et al.*, 2015) and compares the VWC predictions for different sensors. The coefficient of determination investigates the correlation between predicted and observed values. R^2 values range from zero to one, with a perfect fit at one and zero indicating no statistical correlation (Krause *et al.*, 2005).

$$RMSE \; = \; \sqrt{\frac{\sum_{i=i}^{n} \left(VWC_{i,observed} - VWC_{i,predicted}\right)^2}{n}} \tag{8}$$

$$RMSE_r = \sqrt{\frac{\sum_{i=i}^{n}\left(\frac{VWC_{i,observed}-VWC_{i,predicted}}{VWC_{i,observed}}\right)^2}{n}} \times 100\% \tag{9}$$

$$R^2 = \left(\frac{\sum_{i=i}^{n}\left(VWC_{i,observed}-\underline{VWC_{observed}}\right)\left(VWC_{i,predicted}-\underline{VWC_{predicted}}\right)}{\sqrt{\sum_{i=1}^{n}\left(VWC_{i,observed}-\underline{VWC_{observed}}\right)^2}\sqrt{\sum_{i=1}^{n}\left(VWC_{i,predicted}-\underline{VWC_{predicted}}\right)^2}}\right)^2 \tag{10}$$

6 Results and Discussion

The optimum NARX model was able to capture the non-linear dynamics of the moisture variation above different geosynthetic layers. Moreover, the short-term predictions (i.e., 21-days ahead) for VWC values show statistically significant accuracy. The comparison of the state space predictions and NARX predictions is presented in **Fig. 9** for the two GS2 sensors. **Table 3** includes the compared accuracy levels for both techniques. For conciseness, **Fig. 10** shows only the results of NARX predictions developed using GS1-20m and GS3-20m sensory data. The demonstrated high accuracy of short-term VWC predictions supports the applicability of the NARX model as a forecasting technique to plan the mitigation strategies for site-specific geohazards. This approach could be applied to allow forward forecasts in combination with site-specific sensor data.

As shown in **Fig. 9**, the NARX closed-loop predictions of the VWC values for the soil cap above GS2 along with its observed VWCs are depicted against those of the state-space model. Zone 1 represents an initial short wetting period followed by a dry period and a subsequent initial precipitation phase. Zone-2 represents an extended wetting period, with most days having consistent and high precipitation. The NARX network under-predicted VWC values in the dryer period (Zone-1) and over-predicted VWC values in the wetter period (Zone-2). However, the dynamic trends of the GS2-20m VWC values were better captured by the NARX closed-loop in Zone-1. Also, in Zone-2, the predicted values closely follow both the initial increasing trend indicated by the sensors. The lack of precipitation recorded during the period captured in Zone-1 could have resulted in a series of zero-valued exogenous inputs that led to underpredicting VWC values. Similarly, the intermittent yet high-frequency precipitation during the period captured in Zone-2 was inferred by the network to yield high VWC values. Thus, the NARX model has shown high sensitivity to the precipitation events while forecasting the VWC values. Similar to NARX predictions, the state-space model has captured the general trend of the VWC variations. However, the statistical model has under-predicted the VWC values across the board, including the wetting period.

Fig. 9. *Recorded VWC values versus NARX and statistical predictions for sensors located above GS2 composite.*

The majority of low values in both $RMSE$, $RMSE_r$ and R^2 indices in **Table 3** show a higher accuracy of the NARX predictions. The lowest and highest $RMSE's$ (i.e., highest and lowest accuracy) reported for NARX predictions were 0.016 and 0.104, respectively. The NARX prediction errors were distributed with a mean and standard deviation of 0.05 and 0.23, respectively. The model for GS1-20 has a lower accuracy level for the VWC predictions for June and July prediction period in comparison to state-space model predictions for the same month (**Table 3**). However, the differences in these levels are trivial compared to the significant error percentage reported by the state-space model for May, June, and July. The state-space model has limited capabilities in generalizing and considering new parameters for the predictions. Conversely, training the NARX model with more field data and introducing new site-specific parameters can improve the accuracy of the predictions. Moreover, the NARX model has shown greater potential in handling the non-linear dynamics of the VWC variations and hence its higher generalizability compared to the state-space model.

***Table 3**. Accuracy of the predicted VWC using NARX versus statistical model.*

The VWC predictions obtained from NARX closed-loop architecture for the capping layer moisture using GS1 and GS3 sensor data show a close resemblance to the actual values. With the precipitation input being positive values during the wetter period, the NARX model performs well in capturing the variations in the observed VWC data. However, during the dry period (e.g., 4 July to 30 July), the model repeatedly underpredicts the VWC values (**Fig. 10**).

***Fig.10** Recorded VWC values and NARX predictions of VWC values for the capping layer located above GS1 and GS3 composites.*

The predictions of the NARX closed-loop multi-step become less accurate with time (**Fig. 11**). Training the NARX network in open-loop architecture with newly recorded VWC values can improve this for future predictions. As shown in **Fig. 11,** the $RMSE_r$ values of the multi-step predictions have generally increased for the GS1 and GS3. On the contrary, for all prediction periods, the $RMSE_r$ of the GS2 has been less than 10%.

Fig. 11. $RMSE_r$ *for the NARX multi-step predictions of GS1-20 and GS2-20 in different periods.*

7 Prospective

This study demonstrated the successful use of NARX neural network as a data-driven technique to predict the geohazards associated with landfill barriers. Precipitation data collected from a fullscale field study on an existing landfill cap was utilized for training and assessing the model to estimate VWC values within the capping system. Rainfall data has been selected as it is one of the most abundantly available datasets for landfills. The NARX model could predict the short-term variations of the VWC values with reasonable accuracy even when limited datasets are used. The proposed approach was more accurate than the state-space model for most prediction windows.

The performance of landfill is inherently very complex and highly dependent on many parameters that affect the hydrodynamic stability of capping systems. Indeed, the use of the proposed model could be extended for further complexity to be added (should such data be available) beyond that which is reasonable in a deterministic model. The long-term behavior of VWC variations, which depends on many exogenous factors, can be captured by increasing the number of input parameters, NARX hidden layers, and the initial autoregressive time-series memory. Collecting other critical parameters such as material properties, wind patterns, temperature, evapotranspiration, solar radiation, humidity, and age of the construction is necessary for a realistic evaluation of geohazard in landfills. Installing sufficient real-time monitor sensors in well-selected locations, and utilizing smart geosynthetics with embedded sensors, would also enhance the predictions. To this end, larger field data size and extended collection periods are deemed essential to enhance the NARX predictions of the key parameters (e.g., VWC).

Site-specific data can be readily generalized to a broader geographical extent. Data-driven hazard prediction models can also be employed for aging landfill sites that experience adverse climate impacts. With the necessary inputs, NARX is expected to capture long-term predictive trends needed for developing trigger levels and subsequent remedial actions. Holistically, this study highlights the potential of employing a data-driven approach to predict complex field-level behaviors at a low computational cost. The simplicity and reproducibility of the proposed approach are subject candidates for future applications of similar nature.

Notation

A	state matrix
B	input matrix
C	output matrix
D	direct transition matrix
j	Jacobian matrix
H	Hessian matrix
$h(t)$	external input vector (precipitation height)
n	epoch
n_x	number of input layers
n_y	number of output layers
$q(t)$	state vector
r	residual error vector
$RMSE$	root mean squared error
$RMSE_r$	relative root mean squared error
R^2	coefficient of determination
VWC	volumetric water content
w_n	weight vector
λ	scalar variable

References

1. Adamowski, J. and Chan, H.F., 2011. A wavelet neural network conjunction model for groundwater level forecasting. Journal of Hydrology, 407(1-4), pp.28-40.
2. Albright, W.H., Benson, C.H., Gee, G.W., Abichou, T., Tyler, S.W., Rock SA, 2006, Field Performance of Three Compacted Clay Landfill Covers, Vadose Zone Journal Journal 5:1157–1171 (2006).
3. ASTM, 2003. D3385-03 Standard test method for infiltration rate of soils in field using double-ring infiltrometer.
4. Baah-Frempong, E. and Shukla, S.K., 2018. Stability analysis and design charts for a sandy soil slope supporting an embedded strip footing. International Journal of Geo-Engineering, 9(1), pp.1-23.
5. Bergmeir, C. and Benítez, J.M., 2012. On the use of cross-validation for time series predictor evaluation. Information Sciences, 191, pp.192-213.
6. Bergmeir, C., Costantini, M. and Benítez, J.M., 2014. On the usefulness of cross-validation for directional forecast evaluation. Computational Statistics & Data Analysis, 76, pp.132-143.
7. BS 1377 PART 6 - Consolidation and Permeability Tests In Hydraulic Cells And With Pore Pressure Measurement.
8. Bussière, B., Aubertin, M., and Chapuis R. P., 2003. The behaviour of inclined covers used as oxygen barriers. Can. Geotech. J. 40: 512–535
9. Chao, Z., Fowmes, G. and Dassanayake, S.M., 2021. Comparative Study of Hybrid Artificial Intelligence Approaches for Predicting Peak Shear Strength Along Soil-Geocomposite Drainage Layer Interfaces. International Journal of Geosynthetics and Ground Engineering, 7(3), pp.1-19.
10. Choo, L.P. and Yanful, E.K., 2000. Water flow through cover soils using modelling and experimental methods, Journal of Geotechnical and Geoenvironmental Engineering
11. Dassanayake, S. M., and Mousa, A., 2022. Flow dependent constriction-size distribution in gap-graded soils: a statistical inference. Géotechnique Letters 12(1), 46-54.
12. Dassanayake, S.M. and Mousa, A., 2020. Probabilistic stability evaluation for wildlife-damaged earth dams: a Bayesian approach. Georisk: Assessment and Management of Risk for Engineered Systems and Geohazards, 14(1), pp.41-55.
13. Dassanayake, S.M., Mousa, A., Ilankoon, I.M.S.K. and Fowmes, G.J., 2021. Internal instability in soils: a critical review of the fundamentals and ramifications. Transportation Research Record: Journal of the Transportation Research Board.
14. Dassanayake, S.M., Mousa, A., Sheng, L.J. and Chian, C.C., 2020. A statistical inference of hydraulic shear and clogging in internally unstable soils. Géotechnique Letters, 10(1), pp.67-72.
15. Di Nunno, F. and Granata, F., 2020. Groundwater level prediction in Apulia region (Southern Italy) using NARX neural network. Environmental Research, 190, p.110062.
16. Di Nunno, F., Granata, F., Gargano, R. and de Marinis, G., 2021. Prediction of spring flows using non-linear autoregressive exogenous (NARX) neural network models. Environmental Monitoring and Assessment, 193(6), pp.1-17.
17. EN ISO 10776:2012. Geotextiles and geotextile-related products. Determination of water permeability characteristics normal to the plane, under load
18. Gildin, E. and Lopez, T.J., 2011, April. Closed-loop reservoir management: Do we need complex models? In SPE Digital Energy Conference and Exhibition. OnePetro.
19. Guzman, S.M., Paz, J.O. and Tagert, M.L.M., 2017. The use of NARX neural networks to forecast daily groundwater levels. Water resources management, 31(5), pp.1591-1603.
20. Henken-Mellies, U., Gartung, E., 2004. Long-term observation of alternative landfill capping systems – field tests on a landfill in Bavaria. Land Contamination and Reclamation, 12 (1).

21. Jones, D.R.V. and Dixon, N. (2003). Stability of landfill lining systems: Literature Review, Environment Agency Research and Development Project P1-385, Report 1.
22. Khalil, B., Broda, S., Adamowski, J., Ozga-Zielinski, B. and Donohoe, A., 2015. Short-term forecasting of groundwater levels under conditions of mine-tailings recharge using wavelet ensemble neural network models. Hydrogeology Journal, 23(1), pp.121-141.
23. Koerner, R.M. and Soong, T.Y., 2000. Leachate in landfills: the stability issues. Geotextiles and Geomembranes, 18(5), pp.293-309.
24. Krause, P., Boyle, D.P. and Bäse, F., 2005. Comparison of different efficiency criteria for hydrological model assessment. Advances in geosciences, 5, pp.89-97.
25. Leontaritis, I.J. and Billings, S.A., 1985. Input-output parametric models for non-linear systems part I: deterministic non-linear systems. International journal of control, 41(2), pp.303-328.
26. MathWorks, 2020. MATLAB Deep Learning Toolbox Release 2020a. Natick, Massachusetts, United States.
27. Menberg, K., Bayer, P., Zosseder, K., Rumohr, S. and Blum, P., 2013. Subsurface urban heat islands in German cities. Science of the total environment, 442, pp.123-133.
28. Mousa, A., and Youssef, T. A. 2021. Genesis of transitional behaviour in geomaterials: a review and gap analysis. Geomechanics and Geoengineering, 16(4), pp 298-324.
29. Murphy, J. M., D. Sexton D, G. Jenkins G, P. Boorman, B. Booth, K. Brown, R. Clark, M. Collins, G. Harris, E., Kendon *et al.* (2009). UKCP09 Climate change projections science report. July 2nd 2009, MetOffice. Hadley Centre, Exeter, UK. 192p.
30. Nanda, T., Sahoo, B., Beria, H. and Chatterjee, C., 2016. A wavelet-based non-linear autoregressive with exogenous inputs (WNARX) dynamic neural network model for real-time flood forecasting using satellite-based rainfall products. Journal of Hydrology, 539, pp.57-73
31. Narejo, D., 2013. Finite element analysis experiments on landfill cover drainage with geosynthetic drainage layer. Geotextiles and Geomembranes, 38, pp.68-72.
32. Nyhan, J.W., 2005, A Seven-Year Water Balance Study of an Evapotranspiration Landfill Cover. Vadose Zone Journal 4:466–480.
33. Plocoste, T., Jacoby-Koaly, S., Molinié, J. and Petit, R.H., 2014. Evidence of the effect of an urban heat island on air quality near a landfill. Urban Climate, 10, pp.745-757.
34. Raja, M.N.A. and Shukla, S.K., 2021. Predicting the settlement of geosynthetic-reinforced soil foundations using evolutionary artificial intelligence technique. Geotextiles and Geomembranes.
35. Samarasinghe, S., 2016. Neural networks for applied sciences and engineering: from fundamentals to complex pattern recognition. CRC Press.
36. Senevirathne, D.M., Jayasooriya, V.M., Dassanayake, S.M. and Muthukumaran, S., 2021. Effects of pavement texture and colour on Urban Heat Islands: An experimental study in tropical climate. Urban Climate, 40, p.101024.
37. Shukla, S.K. and Kumar, R., 2008. Overall slope stability of prestressed geosynthetic-reinforced embankments on soft ground. Geosynthetics International, 15(2), pp.165-171.
38. Shumway, R.H., Stoffer, D.S. and Stoffer, D.S., 2000. Time series analysis and its applications (Vol. 3). New York: springer.
39. Van Doren, J.F., Van den Hof, P.M., Jansen, J.D. and Bosgra, O.H., 2008. Determining identifiable parameterizations for large-scale physical models in reservoir engineering. IFAC Proceedings Volumes, 41(2), pp.11421-11426.
40. Wanas, N., Auda, G., Kamel, M.S. and Karray, F.A.K.F., 1998, May. On the optimal number of hidden nodes in a neural network. In Conference Proceedings. IEEE Canadian Conference on Electrical and Computer Engineering (Cat. No. 98TH8341), 2, pp. 918-921.

41. Wunsch, A., Liesch, T. and Broda, S., 2018. Forecasting groundwater levels using non-linear autoregressive networks with exogenous input (NARX). Journal of Hydrology, 567, pp.743-758.
42. www.geofabrics.com
43. Zamara, K.A., Dixon, N., Fowmes, G., Jones, D.R.V., Zhang, B., Sharley, M., 2012. Instrumentation measuring hydraulic performance of a landfill cap: Case study. The 5th European Geosynthetics Congress, Valencia 2012.
44. Zamara, K. A., Dixon, N., Fowmes, G., Jones, D. R. V., and Zhang, B., 2014. Landfill side slope lining system performance: A comparison of field measurements and numerical modelling analyses. Geotextiles and Geomembranes, 42(3), 224-235.
45. Zhu, H., Ricote, S., Weddle, P., Jackson, G. and Kee, R.J., 2020, November. Interpreting Electrochemical Impedance Spectra with Physical Models of Mixed-Conducting Protonic Ceramic Electrochemical Cells. In ECS Meeting Abstracts (No. 40, p. 2571). IOP Publishing.
46. Yu, Hao, and Bogdan M. Wilamowski, 2018. "Levenberg–marquardt training." Intelligent systems. CRC Press, 12-1.

Table 1. Hydraulic properties of the geosynthetic layers.

Geosynthetic	Flow [ES ISO 12958] l/m^2/s	In-Place flow capacity, hard-hard platerns @ 20 kPa [ES ISO 11058] l/s/m
GS1	65	n/a
GS2	80	(i = 0.1) 0.5 (i = 1.0) 2.0
GS3	40	(i = 1.0) 0.2

i: applied hydraulic conductivity

Table 2. Parameters of the restoration soil.

Property	Value
Bulk density [Mg/m^3]	1.55
VWC	0.27
Material hydraulic conductivity [m/s]	~10^{-8}
Macro hydraulic conductivity [m/s]	~10^{-5}

Table 3. Accuracy of the predicted VWC using NARX versus state-space model.

Prediction Period	Geosynthetic	$RMSE$		$RMSEr$ (%)		R^2	
		NARX	**State**	**NARX**	**State**	**NARX**	**State**
May to June	GS1-20	0.050	0.1272	7.24	26.6	0.11	0.0133
	GS1-38	0.037	0.079	6.17	25.8	0.643	0.0544
	GS2-20	0.039	0.057	7.32	11	0.134	0.464
	GS2-38	0.032	0.095	4.65	12.95	0.001	0.267
	GS3-20	0.016	0.075	2.56	18.7	0.185	0.376
	GS3-38	0.017	0.029	2.6	7.25	0.167	0.0024
June to July	GS1-20	0.076	0.087	10.33	12.8	0.001	0.2702
	GS1-38	0.026	0.041	4.02	9.44	0.001	0.16743
	GS2-20	0.052	0.034	9.02	5.87	0.274	0.508
	GS2-38	0.035	0.036	4.69	4.57	0.016	0.131
	GS3-20	0.027	0.017	3.96	3.94	0.065	0.471
	GS3-38	0.051	0.140	7.06	18.4	0.043	0.2687
July	GS1-20	0.060	0.09	7.86	13.7	0.535	0.093
	GS1-38	0.072	0.088	12.33	22	0.412	0.1354
	GS2-20	0.059	0.1014	7.86	14.7	0.542	0.057
	GS2-38	0.071	0.043	12.33	5.3	0.412	0.0002
	GS3-20	0.064	0.1	9.32	15.3	0.116	0.00006
	GS3-38	0.104	0.13	15.96	24.8	0.085	0.0462

Fig. 1. Trial sections: a) top surface of the clay barrier; b) installation of the geosynthetic panels; c) spreading the restoration soils; d) completed soil restoration.

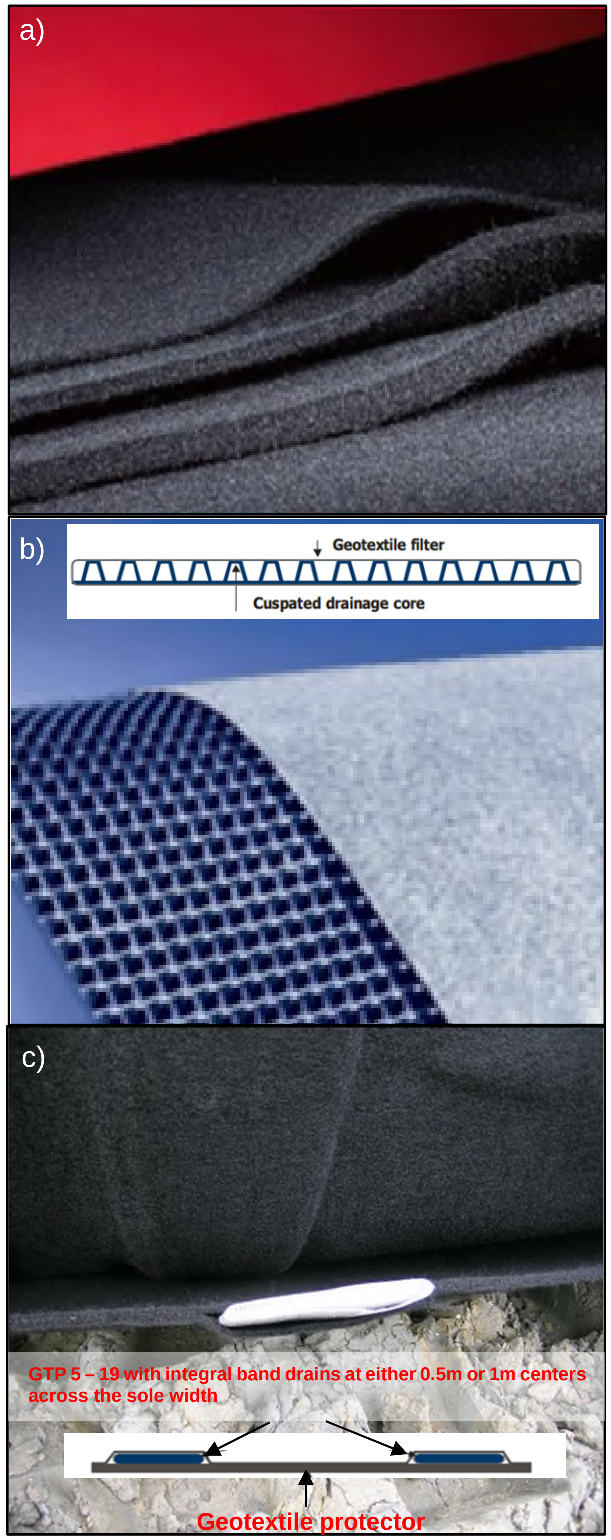

Fig. 2. Geosynthetics used in the trials: a) GS1; non-woven needle-punched geotextile; b) GS2; cuspated core geocomposite; c) GS3; non-woven, needle-punched geotextile with integral longitudinal band drains at regular centers. (www.geofabrics.com).

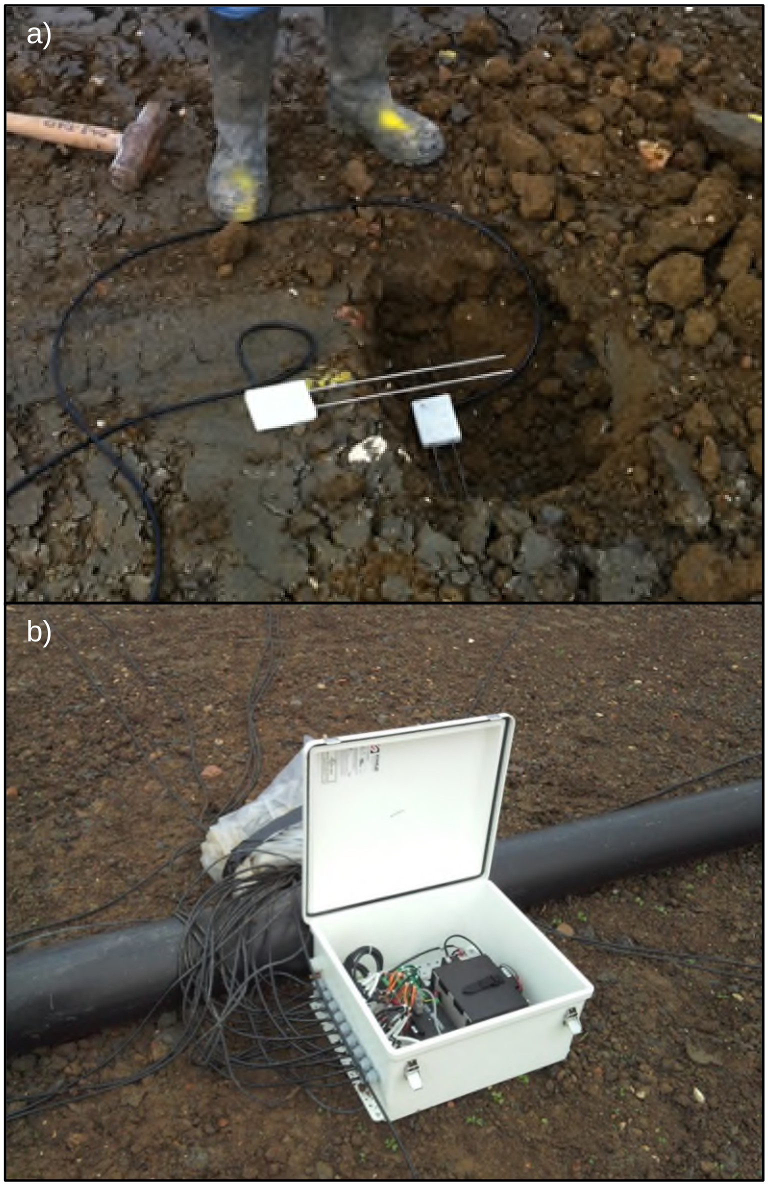

Fig. 3. Installation of VWC sensors in one of the selected locations: (a) two sensors installed at two different levels of the restoration soils capping; (b) logging station.

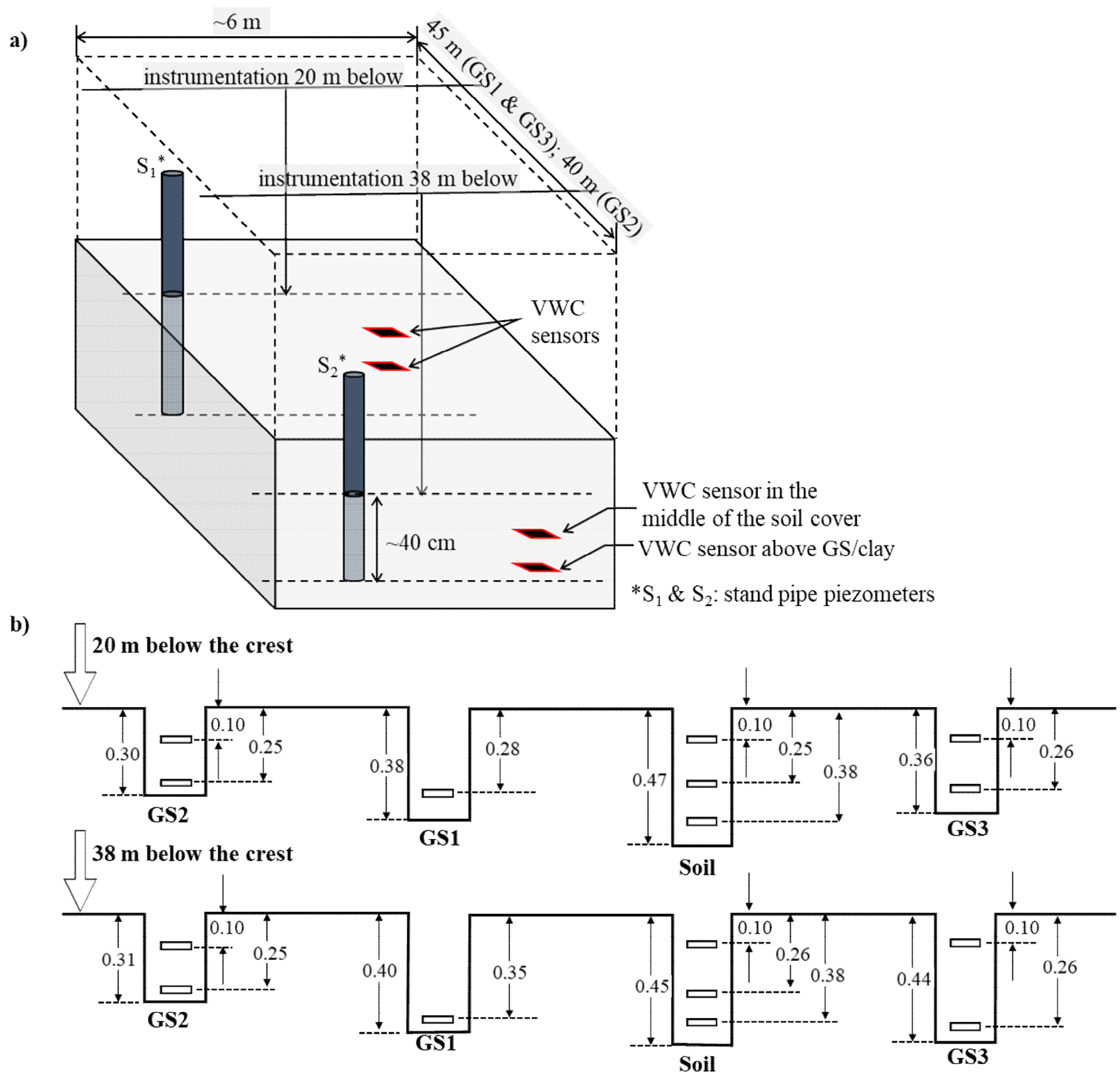

Fig. 4. Volumetric water content (VWC) sensors within the capping system: a) location; b) profile (depth in m). (after Zamara et al. 2012).

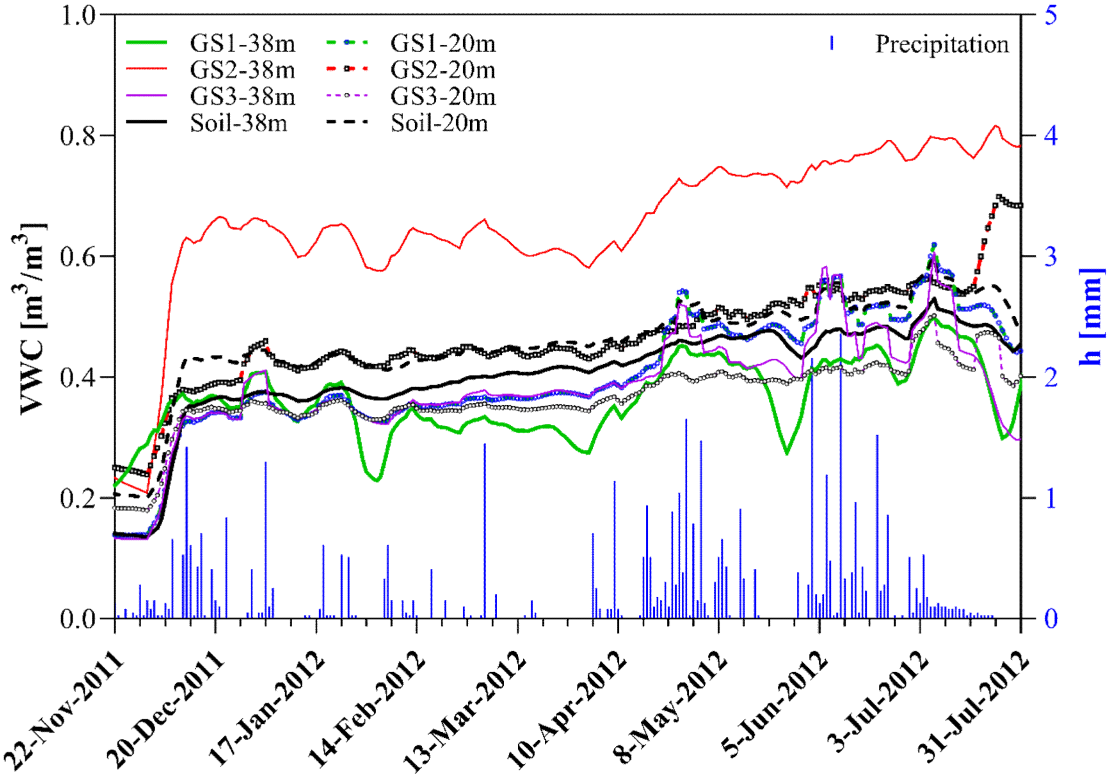

Fig. 5. VWC and precipitation (h) data acquired over the study period (254 days)

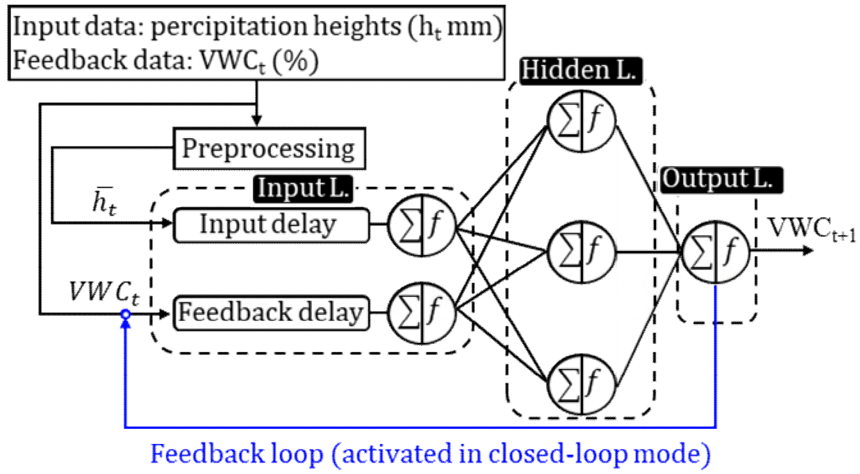

Fig. 6. NARX model with one hidden layer and three hidden nodes, one input time series (h_t), transformed h_t values ($\underline{h_t}$), one output time series (VWC_t), and the feedback loop (activated in closed-loop architecture for multi-step predictions).

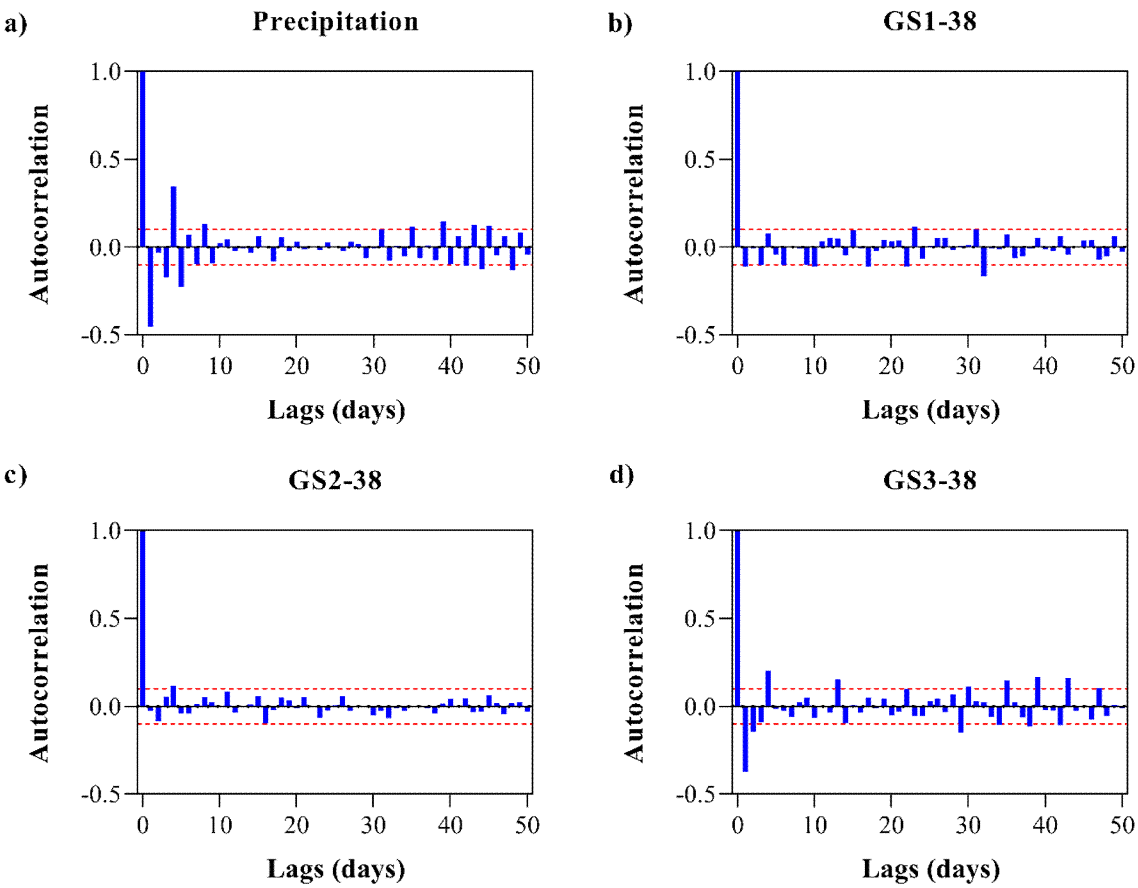

Fig. 7. Autocorrelation of the precipitation and VWC data recorded by the lower sensors (38m below the surface) with 10% confidence interval: a) precipitation data; b) GS1 composite; c) GS2 composite; d) GS3 composite.

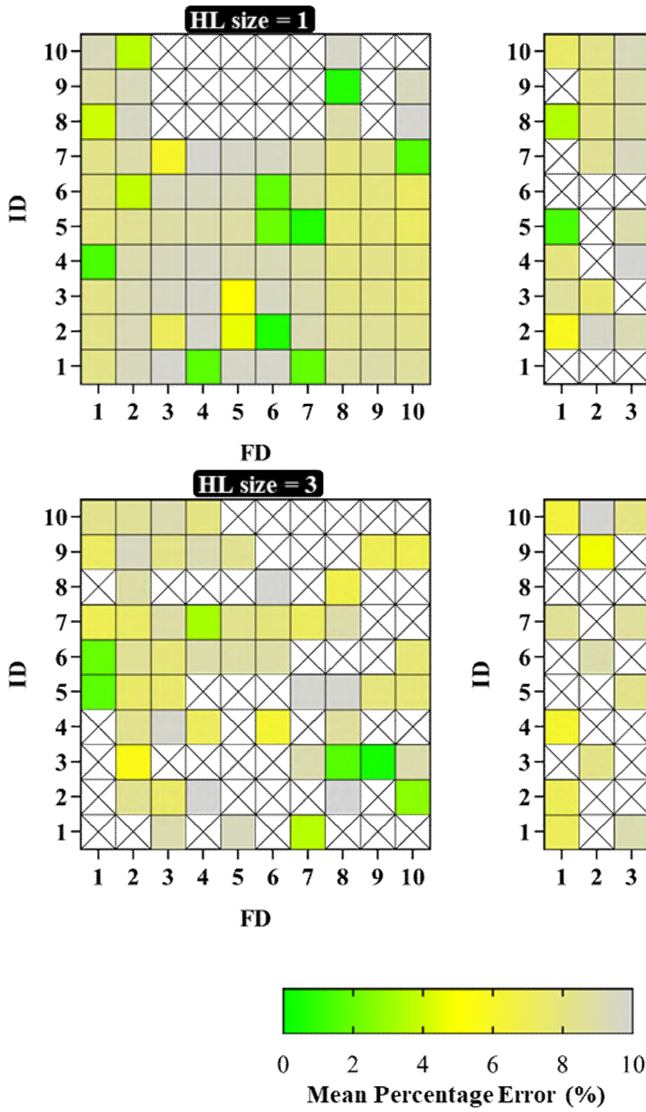

Fig. 8. Average MPE of the prediction performance of the open-loop training by different NARX architectures (the crossed cells indicate an MPE greater than 10%).

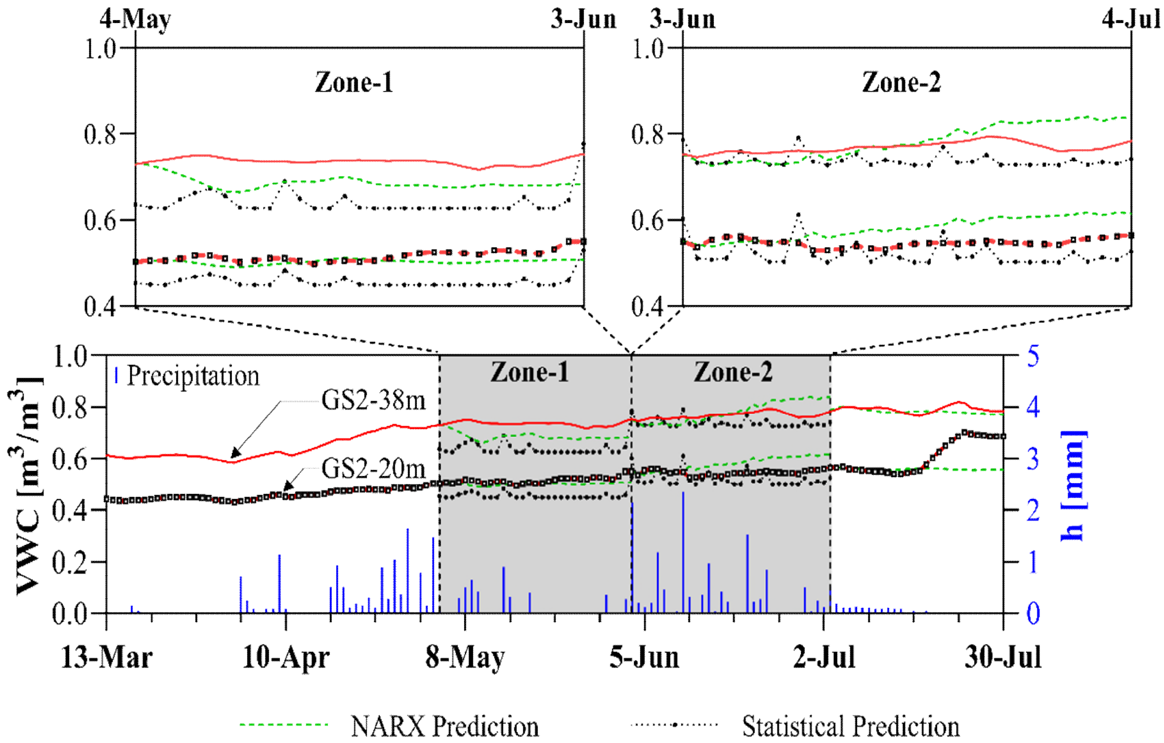

Fig. 9. Recorded VWC values versus NARX and statistical predictions for sensors located above GS2 composite.

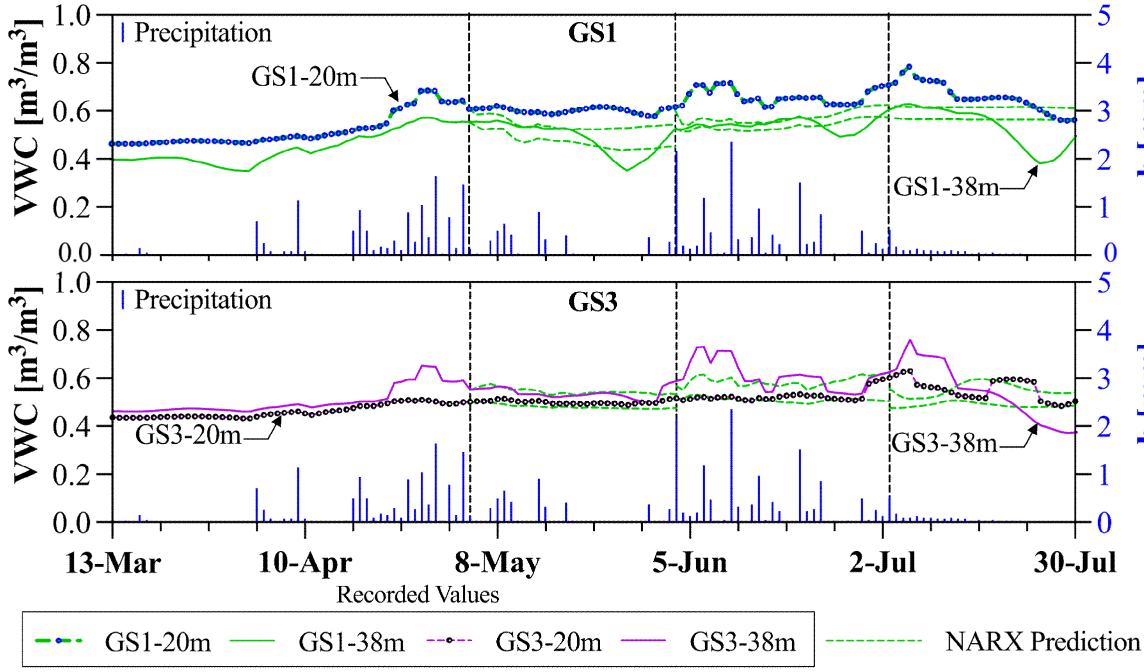

Fig. 10 Recorded VWC values and NARX predictions of VWC values for the capping layer located above GS1 and GS3 composites.

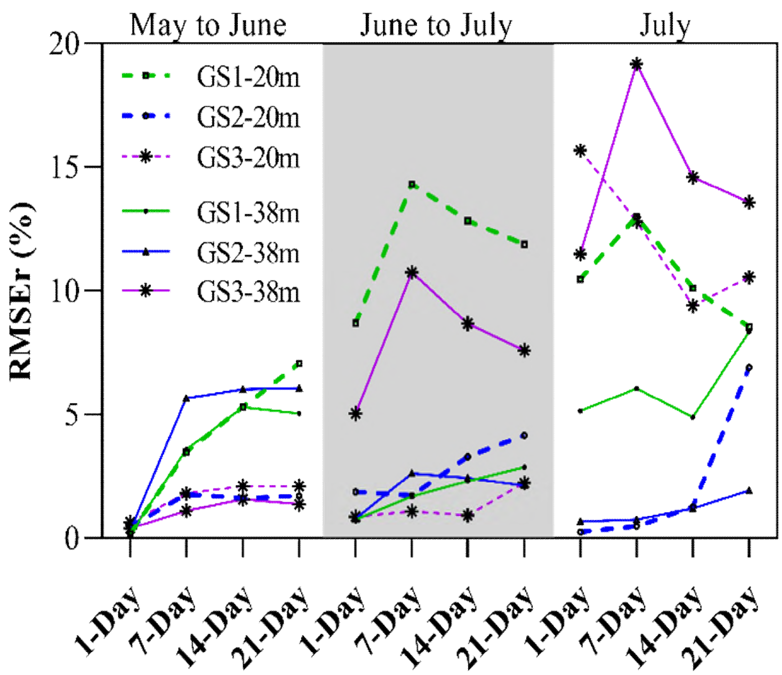

Fig. 11. $RMSE_r$ for the NARX multi-step predictions of GS1-20 and GS2-20 in different periods.